Dating firn cores by vertical strain measurements

Robert L. HAWLEY,[1] Edwin D. WADDINGTON,[1] David L. MORSE,[1,2] Nelia W. DUNBAR,[3] Gregory A. ZIELINSKI[4]

[1]*Department of Earth and Space Sciences, Box 351310, University of Washington, Seattle, Washington 98195-1310, U.S.A.*
E-mail: bo@ess.washington.edu
[2]*Institute for Geophysics, John A. and Katherine G. Jackson School of Geosciences, University of Texas at Austin, Austin, Texas 78712, U.S.A.*
[3]*New Mexico Institute of Mining and Technology, Socorro, New Mexico 87801, U.S.A.*
[4]*Institute for Quaternary and Climate Studies, University of Maine, Orono, Maine 04469-5790, U.S.A.*

ABSTRACT. We have developed a system for measuring a vertical strain-rate profile in the firn on polar ice sheets using a readily available video camera to detect metal bands inserted in an air-filled hole. We used this system in 1995 and 1996 at Taylor Dome, Antarctica. We use density measurements combined with our strain rates to infer vertical velocities. From our velocities we calculate a steady-state depth–age scale for the firn at Taylor Dome. The age of a visible ash layer from 79.1 m is 675 ± 25 years; this ash can be correlated with ash found at 97.2 m in a recent ice core at Siple Dome, West Antarctica.

INTRODUCTION

Firn cores can often be dated by counting annual horizons identified by geochemical analysis. It is useful, however, to have a physically based method of dating these same cores to confirm the geochemical ages, and to resolve any ambiguity in the geochemical interpretation where annual cycles in the chemistry may be poor or non-existent. Where both geochemical and geophysical depth–age relationships exist, they can be compared to extract information on variations in accumulation rate. A physically based model can be derived from a measurement of the rate of vertical compaction in the firn. This measurement is also useful for heat- and ice-flow models.

Making such a measurement is not as straightforward as measuring horizontal motion at the surface, due to problems of access. We have developed a simple method to make this measurement using readily available hardware and software. We track markers placed at intervals in an existing borehole. Unlike previous methods that used a custom-built tuned coil detector to locate markers, we use a commercially available video camera.

TAYLOR DOME

Taylor Dome is an ice dome west of the Transantarctic Mountains on the polar plateau of East Antarctica. First noted by Drewry (1982) in an aerial radio-echo sounding survey of the area, it is centered at 77°50′ S, 159°00′ E, and is the source of ice for Taylor Glacier in the McMurdo Dry Valleys. It is the site of a 554 m ice core to bedrock, taken in the 1993/94 austral summer field season (Fitzpatrick, 1994; Grootes and others, 1994, 2001; Steig and others, 2000). The recovered core contains a record of past climate in its isotopic, chemical, physical and bubble gas properties. In order to interpret the core correctly, studies of the ice dynamics in the region of the drill site were carried out, starting in 1990 (Grootes and others, 1991; Waddington and others, 1991, 1993, 1994; Morse and Waddington, 1992, 1993). A network of over 250 survey poles on the dome was surveyed repeatedly using optical, geoceiver (Transit satellite) and global positioning system (GPS) methods. This network, which was also tied into bedrock points near Taylor Dome and a well-constrained point at McMurdo station, provides horizontal velocity and strain rates on the ice surface (Morse, 1997).

In an effort to further understand the bed topography and the internal structure of the ice in this region, extensive surface-based radio-echo sounding surveys have been made (Morse and Waddington, 1993; Morse, 1997; Morse and others, 1998). These profiles provide accurate bed topography for flow modeling, and also show the internal layering of the ice. Other geochemical and physical studies have been done using the recovered core (Grootes and others, 1994). Three other cores were drilled, varying from 100 to 150 m in depth. One of these holes provided the opportunity to measure vertical motion.

MEASUREMENTS

For our measurements, we used a 130 m deep, 15 cm diameter dry borehole located 50 m from the main hole at Taylor Dome. We placed markers in the hole at approximately 5 m intervals. Each marker is a 10 cm by 1 m strip of sheet phosphor bronze, coiled into a cylinder and released into the hole, where it expands to the size of the hole and holds to the wall by spring tension. A logging tool can pass through these markers. The custom tool used for injecting the bands was built by P. Taylor of Hydro-Tech, based on the recommendations of Raymond and others (1994). Metal bands provide both a sharp edge contrast for video, and a conductive ring geometry that can be exploited by the tuned coil detection system developed by Rogers and LaChapelle (1974), and used at Dyer Plateau by Raymond and others (1996).

https://doi.org/10.3189/172756502781831250 Published online by Cambridge University Press

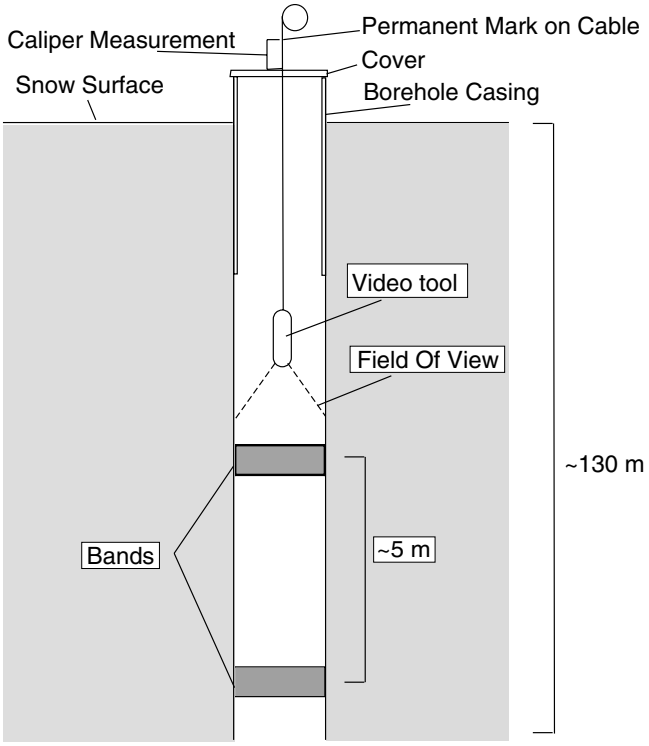

Fig. 1. Schematic of the video tool in the borehole.

Instrument

Our video logging tool is a downward-looking wide-angle video camera with integral light-emitting diodes (LEDs) to provide illumination. This charge-coupled device (CCD) camera is a "SeeSnake" model made by DeepSea Power & Light Inc. We mounted the camera in a simple rigid frame of about 10 cm diameter with tapered ends. We recorded images from the SeeSnake camera with an 8 mm video camcorder.

The tool hangs by a single triaxial cable containing both video and power conductors. We also used the cable to measure the depth of the camera. We ran the cable over a pulley placed atop a survey tripod positioned over the hole. We raised and lowered the tool by hand. A camming cable brake attached to the pulley housing allowed the tool to hang suspended during measurements.

Once the bands were in place, we recorded their relative positions with the video logging tool in January 1995. One year later we repeated the survey. For the first log, we made a permanent mark on the cable when we could image each band. We measured the distance between this mark and the borehole casing with a vernier caliper (see Fig. 1) for this and all subsequent images of this particular band edge.

The two-dimensional image of a band in the hole (Fig. 2) shows the edge of the band as a circle. We determine the location of the camera relative to the band by measuring the observed apparent radius of the band at a given camera position. The distance d between the camera lens and the edge of the band can be expressed in terms of the focal length f of the lens, the actual radius of the band r_a, and the observed radius of the band r_o:

$$d = \frac{f r_a}{r_o} . \quad (1)$$

Ideally we would select an optimum distance from each band to position the camera for caliper measurements, calculate the desired apparent radius r_d for that distance, and make

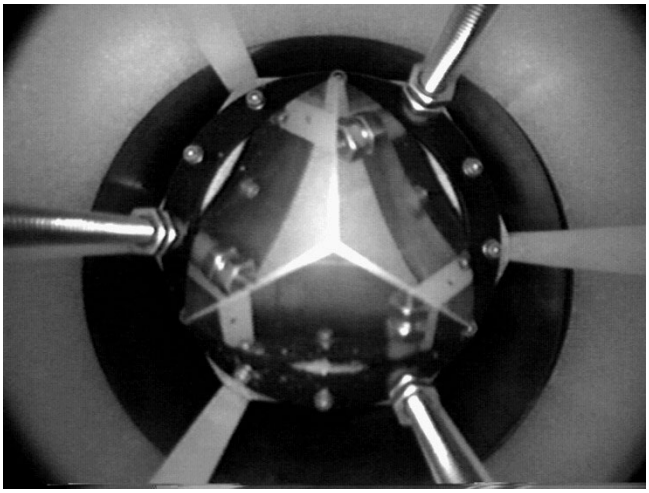

Fig. 2. Downward-looking image of a band at ≈50 m. In the center of the field of view is a corner reflector for looking directly out to the sides which was not used in this analysis. Only the direct image of the band (dark circle) was used.

the caliper measurement when the camera is positioned so that $r_o = r_d$. Since we did not have fine adjustment ability to position our tool, and had no accurate means of assessing the apparent radius in the field, we used the following "bracketing" approach to ensure we had positioned the camera in the same way from year to year.

For each band, we repeated the measurement at least three times, moving the camera vertically by approximately 1 cm each time. The resulting dataset consists of several images of the top and bottom edges of each band, each image taken from a different height above the band. Acquiring multiple images ensured that we could interpolate the measurement to the same distance d relative to the band for each year. Although rearranging and integrating Equation (1) shows that observed apparent radius varies with the inverse square of the distance d, over the short range of our survey the relationship is almost linear.

Data reduction

We first digitized the video images using a commercially available video frame grabber. We then found the radius of the band edge on each video image. Since the band was markedly darker than the surrounding firn, we used an edge-detection process to enhance the edge of the band. After extraneous edges were removed, the apparent radius of the band was determined by fitting a circle to the bright pixels of the band edge, using a least-squares process. For each band, we plotted the apparent radius of the band against the height of the permanent mark on the cable above the top of the borehole casing. The result (Fig. 3) was an almost linear relationship. Repeating the process the following year gave a similar line at a different height. The offset between the two lines gives the displacement of the band relative to our reference mark (i.e. the top of the casing). This displacement divided by the elapsed time between measurements (approximately 1 year) gives relative velocity $w_r(z)$ between the borehole casing and the band at depth z.

Sources of error

Noise appears to grow sharply at depths >85 m. At these depths the decreasing contrast between the ice and band makes the band edge more difficult to distinguish in the video image.

https://doi.org/10.3189/172756502781831250 Published online by Cambridge University Press

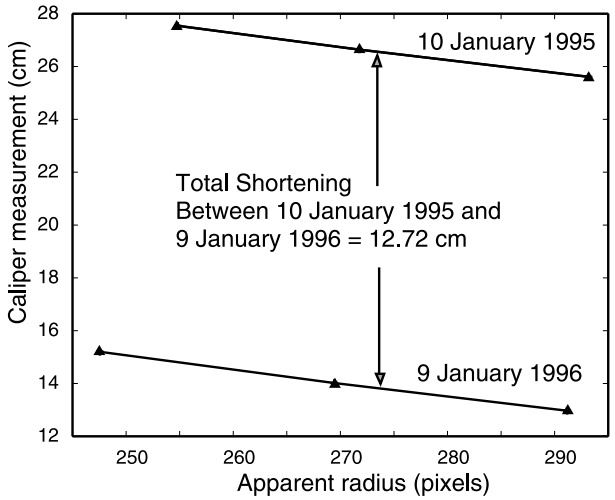

Fig. 3. The observed apparent band-edge radius in an image as a function of position of the logging tool. The caliper measures the distance from a mark on the cable to the top of the borehole casing. Separation between the two lines measures the total shortening of the firn column between 44.58 m and the borehole casing.

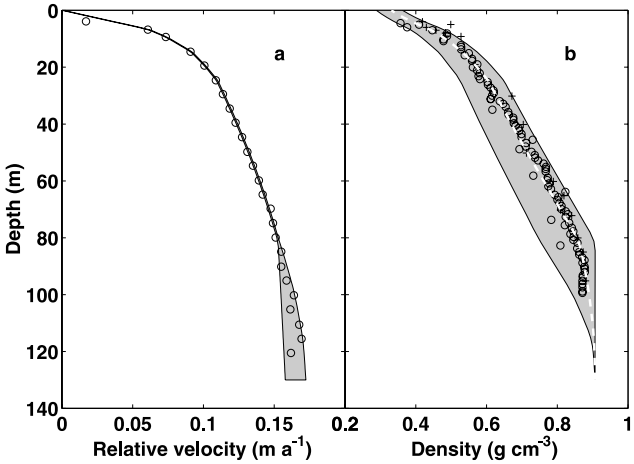

Fig. 4. (a) The measured vertical motion of markers relative to the surface. The shaded grey area indicates the region encompassed by $0 \leq \gamma \leq 1$. (b) A modeled density profile (dashed line) compared to two measured density datasets from a hole 50 m away. The modeled density is constrained to converge on that of pure ice (0.917 g cm^{-3}). The shaded grey area indicates the range of possible density depth profiles for $0 \leq \gamma \leq 1$.

This source of error is addressed in the next section. Modifying the markers to have an easily visible edge would help to overcome this. In addition, since the expected signal for vertical strain becomes very small at these depths, the signal-to-noise ratio declines with depth. Bands such as the ones we used have slipped in past experiments (Raymond and others, 1996). Although we have no reason to conclude that bands were displaced in our experiment, it is impossible to exclude displacements smaller than ±2 mm. A further uncertainty in this system is introduced by the cable. The plastic-sheathed video cable was not designed or tested for consistent elastic or thermal response, and the effects of aging are unknown. If the cable stretches by a certain amount one year and a different amount in a subsequent year, error is introduced. Since the stretch would be affected by the temperature profile along the cable, laboratory tests on the cable are impractical. Using an accurately calibrated logging cable that could carry a video signal would minimize this source of error.

VERTICAL VELOCITY

To obtain a vertical velocity profile for use in calculating a depth–age scale, we must address two issues: accounting for the uncertainty in our measurements, and converting our measured velocities relative to the top of the hole into absolute velocities.

For these calculations, we introduce three assumptions that we will also use in calculating density: (1) the density profile $\rho(z)$ in the hole is in steady state (Sorge's law; Paterson, 1994, p. 14), such that

$$\nabla \cdot (\rho \vec{v}) = 0\,, \qquad (2)$$

(2) $\rho(z)$ is independent of x and y, and (3) the horizontal components of velocity $\vec{v}(x, y, z)$ and therefore the horizontal strain rates are independent of depth z over the depth range of the survey. This last assumption is valid for the shallow depths we are concerned with here, where the largest motions are associated with firn densification. The combined divergence-driven horizontal strain rate, 1.3×10^{-4} a^{-1}, is an order of magnitude smaller than the vertical strain rate (1.3×10^{-3} a^{-1} at 25 m).

Measurement uncertainty

To address the uncertainty in our measurement of $w_\mathrm{r}(z)$ at depth, we define a new parameter γ. We expect a smoothly varying vertical velocity pattern. Below 85 m, our velocity data have a much larger spatial variability than we would expect firn or ice to exhibit. As indicated above, this is likely due to difficulty in distinguishing band edges. A "least-squares" smooth curve through the points might not reflect the true profile. Therefore we use physical constraints to extend our relative velocity curve below the last reliable points. Measured values of horizontal strain at the surface combined with conservation of mass provide a lower limit on the vertical strain rate below 80 m. The magnitude of the vertical strain rate ($|\,\partial w/\partial z\,|$, the slope of the velocity curve) cannot be smaller than the total horizontal strain rate ($|\,\partial u/\partial x + \partial v/\partial y\,|$): unless the firn is dilating, material flowing out in the horizontal direction must be replaced by material from above. The upper limit is taken as a curve drawn through our highest relative velocity measurements. The true vertical velocity profile is then somewhere between the two extremes. We define the partitioning coefficient $\gamma, 0 \leq \gamma \leq 1$ as a measure of the position of the actual velocity profile $w_\mathrm{r}(z)$ relative to the two extremes. Once a value of γ is chosen,

$$w_\mathrm{r}(z) = \gamma w_\mathrm{r}^\mathrm{l}(z) + (1-\gamma) w_\mathrm{r}^\mathrm{u}(z)\,, \qquad (3)$$

where $w_\mathrm{r}^\mathrm{l}(z)$ and $w_\mathrm{r}^\mathrm{u}(z)$ are the lower and upper limits, respectively. The measured $w_\mathrm{r}(z)$ data points, and the range of $w_\mathrm{r}(z)$ profiles allowed by Equation (3) are shown in Figure 4a. A sampling of the measured w_r values are listed in Table 1, along with measured densities.

Absolute velocity

Our goal is to arrive at a true vertical velocity for each surveyed point in the borehole, to be used in calculating a depth–age scale. For any given marker, the true vertical velocity is found by adding the measured velocity $w_\mathrm{r}(z)$ relative to the surface marker to the absolute downward velocity w_o of the surface marker. For a steady surface, ideally we

https://doi.org/10.3189/172756502781831250 Published online by Cambridge University Press

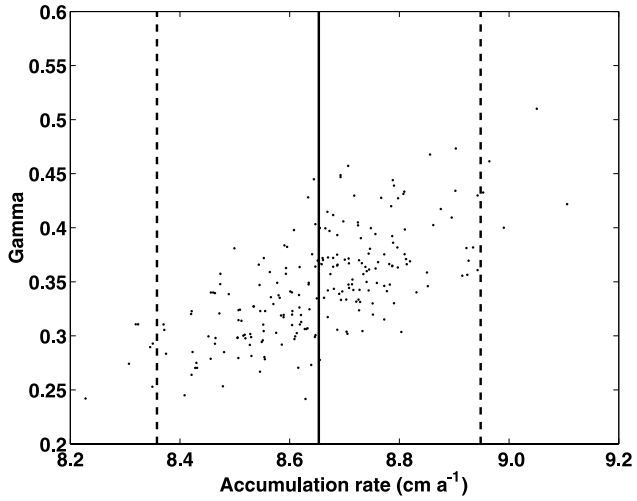

Fig. 5. The population of 224 "bootstrapped" $\dot{b}$ and γ, the best-fit $\dot{b}$ (solid vertical line) and 95% confidence interval on $\dot{b}$ (dashed vertical lines). $\dot{b}$ is indicated in ice equivalent units.

could measure w_o using survey-quality repeat GPS measurements such as those made by Hamilton and Whillans (1996). Since we do not have such data, we infer w_o using measured density profiles from the main core site 50 m away.

Conservation of mass in a vertical column of ice from the surface to the depth z_{bot} of the borehole (here 130 m) gives

$$w_o\rho_o - w(z_{bot})\rho(z_{bot}) = \left(\frac{\partial u}{\partial x}+\frac{\partial v}{\partial y}\right)\int_0^{z_{bot}}\rho(z)\,dz\,, \quad (4)$$

where ρ_o is the density of snow at the top of the hole. Fitzpatrick (1994) and Grootes and others (1994) measured density ρ as a function of depth z, and Morse (1997) measured the horizontal strain rate $(\partial u/\partial x + \partial v/\partial y)$ at the surface using a network of poles. Equation (4) says that in steady state any mass that comes in the top of the box, and does not go out the sides, must come out the bottom.

Now, to express w_o entirely in terms of readily measurable quantities, we first recognize that $w_o = w(z_{bot}) - w_r(z_{bot})$, where we have already measured the relative velocity $w_r(z_{bot})$ of the bottom of the hole. Second, we note that the mass flux $w_o\rho_o$ through the upper surface of the ice sheet can also be written as $\dot{b}\rho_{ice}$, where $\dot{b}$ is ice-equivalent accumulation rate, and ρ_{ice} is the density of ice. Third, we note that the density $\rho(z_{bot})$ at the bottom of the hole has reached the ice density ρ_{ice}. Incorporating this information into Equation (4) leads to

$$w_o = \dot{b} - \frac{1}{\rho(z_{bot})}\left(\frac{\partial u}{\partial x}+\frac{\partial v}{\partial y}\right)\int_0^{z_{bot}}\rho(z)dz - w_r(z_{bot})\,. \quad (5)$$

We then use $\dot{b}$ and γ as free parameters in the density model described below.

Table 1. Values of relative velocity w_r and density measurements ρ_1 from Fitzpatrick (1994) and ρ_2 from Grootes and others (1994). Final accepted $w(z)$ and expected w_ρ predicted by steady state and Sorge's law are also shown

Depth m	w_r m a^{-1}	ρ_1 g cm^{-3}	ρ_2 g cm^{-3}	w m a^{-1}	w_ρ m a^{-1}
3.87	0.017	–	–	0.203	–
9.41	0.073	0.529	0.485	0.165	0.166
19.43	0.101	0.573	0.569	0.138	0.138
29.44	0.114	0.665	0.618	0.124	0.124
39.52	0.123	0.702	0.677	0.115	0.114
49.82	0.131	0.713	0.727	0.107	0.104
59.84	0.139	0.788	0.771	0.099	0.096
69.77	0.148	0.807	0.811	0.092	0.090
79.94	0.151	0.856	0.846	0.086	0.086
90.16	0.155	0.870	0.877	0.083	0.083
100.21	0.164	0.884	0.871	0.080	0.080
110.55	0.168	–	–	0.078	–
120.51	0.162	–	–	0.077	–

Density profile

Since the firn is compressible, vertical velocity is coupled to firn compaction. We find w_o by selecting the pair of parameters $[\dot{b}, \gamma]$ that, when combined with our measured dw/dz and used in the calculations below, simultaneously produces a pair of coupled solutions $w(z)$ and $\rho(z)$ such that $\rho(z)$ best matches measured densities. We then accept that corresponding velocity solution $w(z)$.

Expanding Equation (2) with the assumptions above and then solving for $\partial\rho/\partial z$ yields

$$\frac{\partial\rho}{\partial z} = -\left(\frac{\partial u}{\partial x}+\frac{\partial v}{\partial y}+\frac{\partial w}{\partial z}\right)\frac{\rho(z)}{w(z)} \quad (6)$$

which can be integrated numerically to obtain a density profile, using measured values of $\partial u/\partial x$, $\partial v/\partial y$ and $\partial w/\partial z$. We computed density distributions using a range of possible values for both $\dot{b}$ and γ. For each $[\dot{b}, \gamma]$ pair, we compared the modeled density profile to measured density data from the main borehole 50 m away (Fitzpatrick 1994; Grootes and others, 1994). Our preferred profile is the one that matches the measurements most closely in a least-squares sense. Equation (6) can also be solved to predict a $w(z)$ profile, based on a measured $\rho(z)$ profile and a surface velocity. Using a value for the surface velocity from our final accepted velocity profile (derived in this section), the resulting velocity profile w_ρ agrees well with our accepted final $w(z)$ profile; both can be seen in Table 1. To quantify our confidence in our preferred profile, we use the "bootstrap" method (Press and others, 1992, p. 691).

Bootstrapping confidence levels

The goal of bootstrapping is to place confidence bounds on a measurement or on a calculated result, where the underlying sampled population cannot provide traditional statistical information. In the current situation, we look for confidence bounds on our calculated $w(z)$ and $\rho(z)$, yet we have only one density sample from any given depth and therefore cannot calculate a standard deviation for these underlying data. In the bootstrap method, the lack of repeated measurements is compensated for by using the actual dataset D_0 to create a number of synthetic datasets $D_1, D_2, ...$, each with the same number of points as the original set. Each synthetic dataset is populated by drawing samples at random from the measured dataset *with replacement*. Replacement ensures that in the synthetic datasets some measurements will be repeated (and thus be more highly weighted) and some will be omitted. For each of these synthetic datasets we find a "best-fit" calculated density profile. The resulting set of "best-fit" values of $\dot{b}$ and γ serve as a population from which we can calculate meaningful statistics. One such population of 224 sets of fitted parameters is shown in Figure 5, along with our resulting preferred value for $\dot{b}$ and its 95% confidence interval. This confidence interval

https://doi.org/10.3189/172756502781831250 Published online by Cambridge University Press

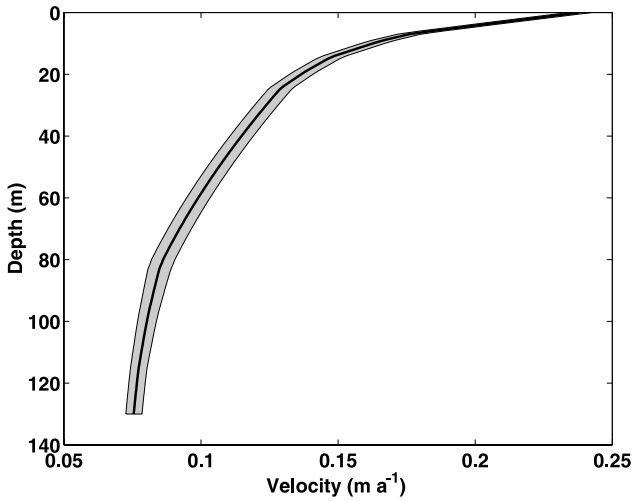

Fig. 6. The vertical velocity profile. The bold line shows the best fit. The shaded region contains all profiles with $\dot{b}$ inside the 95% confidence interval in Figure 5.

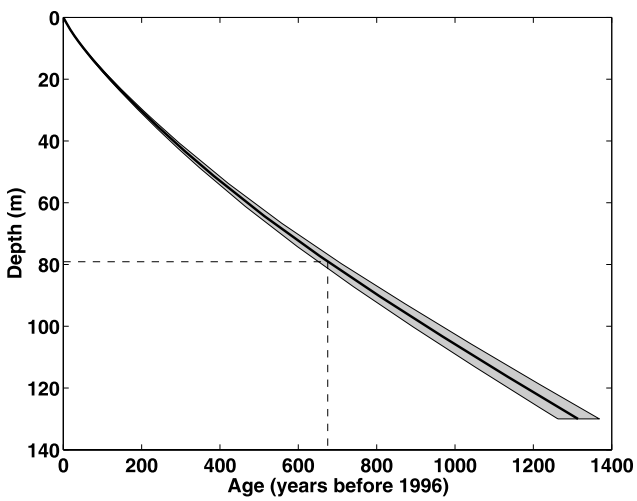

Fig. 7. Depth–age scale for the firn at Taylor Dome C hole. The bold curve was made using the preferred accumulation of 8.65 cm a^{-1} and γ of 0.35. The shaded region represents the range of possible depth–age scales with $\dot{b}$ inside the 95% confidence interval in Figure 5. The depth and age of a volcanic ash layer from a depth of 79.1 m (675 ± 25 years) are indicated by the dashed lines.

is used to estimate the error range on the velocity profile and the associated depth–age scale discussed below.

The preferred velocity profile, shown by the bold curve in Figure 6, uses $\dot{b} = 8.65\,\mathrm{cm\,a^{-1}}$ and $\gamma = 0.35$. The shaded region contains all profiles with $\dot{b}$ inside the 95% confidence interval in Figure 5.

Surface density measurements provide further support of our optimization. All model runs within our 95% confidence interval produced surface densities in the range $0.32\,\mathrm{g\,cm^{-3}} \leq \rho \leq 0.35\,\mathrm{g\,cm^{-3}}$; these values fall within the range of measured surface densities at Taylor Dome (M. Duvall, unpublished field report, 1994).

DATING THE CORE

We use the vertical velocity profile in Figure 6 to calculate a depth–age scale for the upper 130 m, following the procedure used by Paterson and others (1977) for Devon Ice Cap, Canadian Arctic. We still assume that the vertical velocity profile is in steady state in a reference frame fixed to the surface, which could be moving up or down. Although the particle paths do not follow straight down the borehole, the horizontal components of $\vec{v}(x, y, z)$ are small enough that the vertical component is unlikely to vary with x or y and the one-dimensional approximation is valid.

We numerically integrate the inverse of the vertical velocity from the surface to depth z to find the age today of ice at depth z,

$$\mathrm{age} = \int_0^z \frac{1}{w(\xi)}\,\mathrm{d}\xi\,. \qquad (7)$$

Using our preferred $w(z)$ profile, the resulting depth–age profile is shown by the bold curve in Figure 7. The shaded region on either side of the bold curve represents age profiles produced with the highest and lowest w_o values allowed by our 95% confidence interval in Figure 5.

DISCUSSION

Accumulation rates

The range of accumulation rates within the 95% confidence interval in Figure 5 is compatible with local accumulation rates measured by a variety of methods (Morse and others, 1999). Our measurement provides a physical constraint on the average accumulation rate over the last 1300 years, in much the same way as gross-β measurements of nuclear bomb fallout products (see Picciotto and Wilgain (1963) for a description of the method) provide a constraint on average accumulation over the last ≈45 years.

Our 1300 year average value for $\dot{b}$ is greater than the 45 year average of $\dot{b} = 7.6\,\mathrm{cm\,a^{-1}}$ from gross-β, and greater than the average of ≈6–7 $\mathrm{cm\,a^{-1}}$ over the Holocene (Morse and others, 1998; Steig and others, 2000). Conservation of mass implies that a steady-state ice dome with $\dot{b}$ throughout the Holocene equal to our value of $8.65\,\mathrm{cm\,a^{-1}}$ would require a larger horizontal flux divergence, either by being considerably thicker than Taylor Dome, or having greater horizontal strain rates than those measured by Morse (1997).

This illustrates the temporal variability of the accumulation-rate pattern at Taylor Dome. Our analysis derives an average value of $\dot{b}$, whereas the true accumulation rate probably varied over time. Since the accumulation rate affects the slope of the depth–age curve, a calculation that allowed for a time-dependent accumulation rate would produce a depth–age profile which might show slope deviations of up to 10–20% from our preferred curve in Figure 7, but would on average produce similar ages at similar depths.

Ash layer

A number of primary volcanic ash, or tephra, layers are found in the ice cores from Taylor Dome and from Siple Dome, West Antarctica. Tephra layers, when found in sedimentary sequences such as ice, provide time-stratigraphic markers because volcanic eruptions, ash transport and deposition occur in geologically short time intervals. A well-defined and chemically distinctive tephra layer is found at 79.2 m depth in the Taylor Dome ice core. Although this layer is interpreted to be from a local source volcano and cannot be directly dated, it is chemically indistinguishable from a layer found at 97.2–97.7 m depth in the Siple Dome B core. Based on the geochemical correlation, as well as the similarity of shard morphology, these layers are interpreted to be the result of

https://doi.org/10.3189/172756502781831250 Published online by Cambridge University Press

the same volcanic eruption, and therefore to represent the same time interval in the two cores.

The age of the lowest horizon where the ash was found, 97.7 m depth, in the Siple Dome A ice core has been estimated to be 709 years before 1995 with an error of 10% (personal communication from K. Taylor, 2001), and we would infer that the 79.2 m depth in the Taylor Dome core is the same age. This age is very close to the age determined by vertical strain measurements presented in this paper (675 ± 25 years before 1996; Fig. 7). The slight discrepancy between the ages may be in part due to small errors in the age–depth estimates for the Siple Dome ice core.

CONCLUSIONS

Measurement of vertical velocity in an ice-sheet borehole is possible with readily available hardware and software that can be used with few modifications. This is a useful measurement because it can provide a physically based depth–age scale where the geochemical annual layer record is disturbed or unresolvable. Our calculated depth–age scale is likely the most accurate depth–age scale for the Taylor Dome firn thus far, and can also help constrain dating of the Siple Dome core.

ACKNOWLEDGEMENTS

We thank H. Conway and J. Bailey for help with field measurements, T. Gades and K. Cuffey for help with data processing, P. Taylor for equipment fabrications, and N. Humphrey for introducing us to the SeeSnake video camera. J. Meyssonnier (Scientific Editor), M. Funk and T. Pfeffer provided helpful comments that improved the manuscript. The hole was drilled by the Polar Ice Coring Office, and logistical support was provided by Antarctic Support Associates. This work was supported by the U.S. National Science Foundation through grants OPP-9221261 and OPP-9421644, and by the Mary Gates Foundation with a Research Training Grant to R.L.H.

REFERENCES

Drewry, D. J. 1982. Ice flow, bedrock, and geothermal studies from radio-echo sounding inland of McMurdo Sound, Antarctica. *In* Craddock, C., *ed. Antarctic geoscience.* Madison, WI, University of Wisconsin Press, Abstract, 977–983.

Fitzpatrick, J. J. 1994. Preliminary report on the physical and stratigraphic properties of the Taylor Dome ice core. *Antarct. J. U.S.*, **29**(5), Review 1994, 84–86.

Grootes, P. M., E. J. Steig and C. Massey. 1991. "Taylor ice-dome" study: reconnaissance 1990–1991. *Antarct. J. U.S.*, **26**(5), Review 1991, 79–81.

Grootes, P. M., E. J. Steig and M. Stuiver. 1994. Taylor ice dome study 1993–1994: an ice core to bedrock. *Antarct. J. U.S.*, **29**(5), Review 1994, 79–81.

Grootes, P. M., E. J. Steig, M. Stuiver, E. D. Waddington, D. L. Morse and M.-J. Nadeau. 2001. The Taylor Dome study Antarctic ^{18}O record and globally synchronous changes in climate. *Quart. Res.*, **56**(5), 289–298.

Hamilton, G. S. and I. M. Whillans. 1996. Global positioning system measurements of ice-sheet mass balance using the "coffee-can" method. *Antarct. J. U.S.*, **31**(2), Review 1996, 86–88.

Morse, D. L. 1997. Glacier geophysics at Taylor Dome, Antarctica. (Ph.D. thesis, University of Washington.)

Morse, D. L. and E. D. Waddington. 1992. Glacier geophysical studies for an ice-core site at Taylor Dome: year two. *Antarct. J. U.S.*, **27**(5), Annual Review 1992, 59–61.

Morse, D. L. and E. D. Waddington. 1993. Glacier geophysical studies at Taylor Dome: year three. *Antarct. J. U.S.*, **28**(5), Review 1993, 67–69.

Morse, D. L., E. D. Waddington and E. J. Steig. 1998. Ice age storm trajectories inferred from radar stratigraphy at Taylor Dome, Antarctica. *Geophys. Res. Lett.*, **25**(17), 3383–3386.

Morse, D. L. *and 7 others*. 1999. Accumulation rate measurements at Taylor Dome, East Antarctica: techniques and strategies for mass balance measurements in polar environments. *Geogr. Ann.*, **81A**(4), 683–694.

Paterson, W. S. B. 1994. *The physics of glaciers. Third edition.* Oxford, etc., Elsevier.

Paterson, W. S. B. *and 7 others*. 1977. An oxygen-isotope climatic record from the Devon Island ice cap, Arctic Canada. *Nature*, **266**(5602), 508–511.

Picciotto, E. and S. Wilgain. 1963. Fission products in Antarctic snow, a reference level for measuring accumulation. *J. Geophys. Res.*, **68**(21), 5965–5972.

Press, W. H., S. A. Teukolsky, W. T. Vetterling and B. P. Flannery. 1992. *Numerical recipes in C: the art of scientific computing. Second edition.* Cambridge, Cambridge University Press.

Raymond, C. F., J. C. Rogers, P. L. Taylor and B. Koci. 1994. Vertical strain measurement in core holes. *Natl. Inst. Polar Res. Mem., Special Issue* 49, 234–240.

Raymond, C., B. Weertman, L. Thompson, E. Mosley-Thompson, D. Peel and B. Mulvaney. 1996. Geometry, motion and mass balance of Dyer Plateau, Antarctica. *J. Glaciol.*, **42**(142), 510–518.

Rogers, J. C. and E. R. LaChapelle. 1974. The measurement of vertical strain in glacier bore holes. *J. Glaciol.*, **13**(68), 315–319.

Steig, E. J. *and 7 others*. 2000. Wisconsinan and Holocene climate history from an ice core at Taylor Dome, western Ross Embayment, Antarctica. *Geogr. Ann.*, **82A**(2–3), 213–235.

Waddington, E. D., D. Morse, M. J. Balise and J. Firestone. 1991. Glacier geophysical studies for an ice core site at "Taylor Dome". *Antarct. J. U.S.*, **26**(5), Review 1991, 71–73.

Waddington, E. D., D. L. Morse, P. M. Grootes and E. J. Steig. 1993. The connection between ice dynamics and paleoclimate from ice cores: a study of Taylor Dome, Antarctica. *In* Peltier, W. R., *ed. Ice in the climate system.* Berlin, etc., Springer-Verlag, 499–516. (NATO ASI Series I: Global Environmental Change 12.)

Waddington, E. D., D. L. Morse and G. D. Clow. 1994. Glacier geophysics at Taylor Dome: year 4. *Antarct. J. U.S.*, **29**(5), Review 1994, 82–84.

MS received 5 December 2001 and accepted in revised form 18 June 2002